

Interaction of Polymers with Enzalutamide Nanodroplets—Impact on Droplet Properties and Induction Times

Venecia R. Wilson, Naila A. Mugheirbi, Laura I. Mosquera-Giraldo, Alexandru Deac, Dana E. Moseson, Daniel T. Smith, Diana C. Novo, Carlos H. Borca, Lyudmila V. Slipchenko, Kevin J. Edgar, and Lynne S. Taylor*

Cite This: *Mol. Pharmaceutics* 2021, 18, 836–849

Read Online

ACCESS |

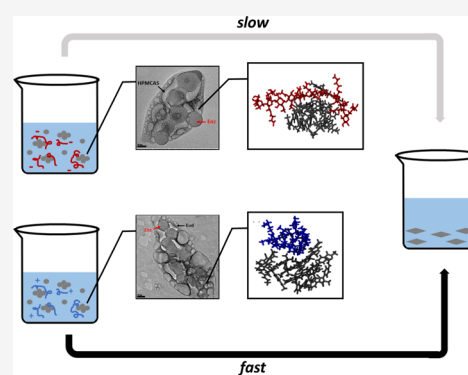
Metrics & More

Article Recommendations

Supporting Information

ABSTRACT: Amorphous solid dispersions (ASDs), which consist of a drug dispersed in a polymeric matrix, are increasingly being applied to improve the *in vivo* performance of poorly water-soluble drugs delivered orally. The polymer is a critical component, playing several roles including facilitating drug release from the ASD, as well as delaying crystallization from the supersaturated solution generated upon dissolution. Certain ASD formulations dissolve to produce amorphous drug-rich nanodroplets. The interaction of the polymer with these nanodroplets is poorly understood but is thought to be important for inhibiting crystallization in these systems. In this study, the impact of ionic polymers on the crystallization kinetics of enzalutamide from supersaturated solutions containing different amounts of amorphous nanodroplets was evaluated by determination of nucleation induction times. The amount of the polymer associated with the drug nanodroplets was also determined. When comparing two polymers, hydroxypropylmethyl cellulose acetate succinate (HPMCAS) and Eudragit E PO, it was found that the crystallization tendency and physical properties of the drug nanodroplets varied in the presence of these two polymers. Both polymers distributed between the aqueous phase and the drug-rich nanodroplets. A greater amount of Eudragit E PO was associated with the drug-rich nanodroplets. Despite this, Eudragit E PO was a less-effective crystallization inhibitor than HPMCAS in systems containing nanodroplets. In conclusion, in supersaturated solutions containing amorphous nanodroplets, the extent of association of a polymer with the drug nanodroplet does not solely predict crystallization inhibition.

KEYWORDS: crystallization kinetics, drug-rich nanodroplet, polymer–drug interaction, amorphous solid dispersion



INTRODUCTION

Over the past decade, there has been increasing interest in gaining an improved mechanistic understanding of the enhanced *in vivo* performance often observed for amorphous solid dispersions (ASDs) as compared to the crystalline drug and, in some instances, other solubility-enhancing formulations. This interest has been driven by the large number of poorly aqueous soluble drugs in development.¹ For ASDs, the main excipient combined with the drug is a polymer, and in some instances, a surfactant is added.² The role of the polymer is to inhibit crystallization of the amorphous drug from the solid formulation during storage to facilitate drug release and, for many drugs, to delay crystallization from the supersaturated solution generated upon dissolution. The latter property is particularly important for drugs that crystallize from solution over biologically relevant time frames. Surfactants are typically added to improve processing and/or drug release.

Ideally, ASD dissolution is rapid relative to the rate of absorption across the gastrointestinal membrane and leads to the formation of a supersaturated solution. Supersaturation is known to drive membrane transport.³ If the concentration of the

drug in solution is below the amorphous solubility, that is, below the maximum achievable free drug concentration, the system contains a dissolved polymer and drug. However, if the ASD dissolves to reach a concentration that exceeds the amorphous solubility, amorphous nanodroplets can form as a result of liquid–liquid or glass–liquid phase separation (LLPS or GLPS).^{4–8} LLPS occurs if the resultant amorphous nanodroplets are above their glass transition temperature (T_g), whereas the process is termed GLPS if the nanodroplets are glassy (below their T_g). It is desirable that the drug undergoes LLPS/GLPS following release from the ASD since the nanodroplets that form in solution can act as a depot, thus rapidly replacing the drug transferred across the membrane,

Received: August 12, 2020

Revised: January 25, 2021

Accepted: January 26, 2021

Published: February 4, 2021



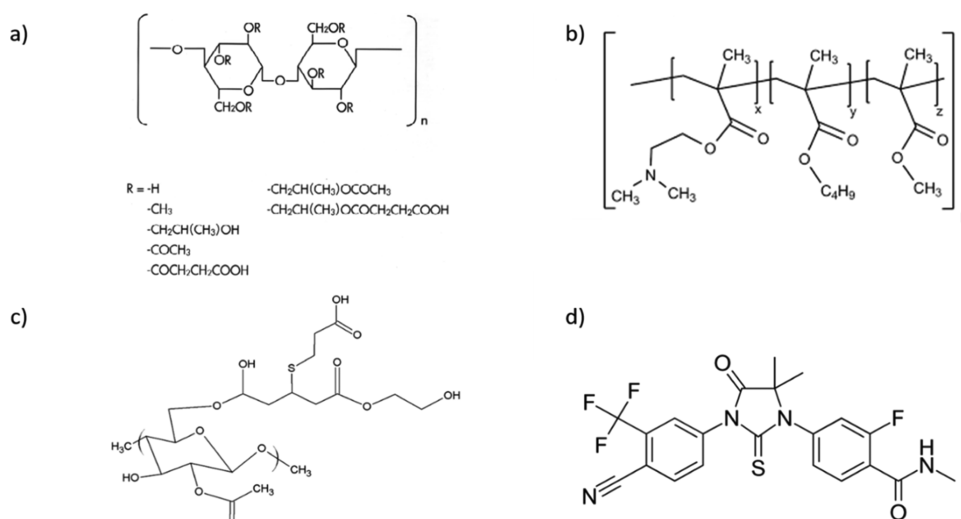


Figure 1. Structures of (a) HPMCAS, (b) Eudragit E PO, (c) P177, and (d) enzalutamide.

maintaining the supersaturation at a maximum value, and leading to high and sustained membrane flux.^{6–8} Nonetheless, the *in vivo* benefits of the nanodroplets can only be realized if crystallization can be avoided. Consequently, ASD dissolution is a complex process since the drug can undergo different phase transformations and exist in several different speciation states such as molecularly dissolved drug, nanodroplets, undissolved ASD particles, or as a crystalline form.⁸

In a solution containing nanodroplets, the chemical potential of the drug in the nanodroplet and in the bulk solution phase is equivalent and is higher than that for the corresponding crystal.⁹ Hence, there is a driving force for crystallization, and crystallization can occur from either the nanodroplets or drug present in the aqueous-rich phase or at the interface of the two phases. Given the important role of the polymer as a crystallization inhibitor, it is critical to understand the distribution of the polymer between the bulk aqueous solution and the nanodroplets. Raina et al. demonstrated that chemically diverse polymers showed variations in their distribution between the aqueous phase and the drug-rich nanodroplets, noting that the polymer distribution trended with the polymer hydrophobicity; hydrophilic polymers were found predominantly in the aqueous phase, and amphiphilic polymers distributed between both phases while hydrophobic polymers were mainly present in the drug-rich phase.¹⁰ They further noted that polymers that were effective crystallization inhibitors distributed between both aqueous and drug-rich phases. Ueda et al. made a similar observation when studying a group of chemically related polymers and suggested that the extent of crystallization inhibition was related to the amount of the polymer associated with the amorphous drug nanodroplets.¹¹ More recently, Wang et al. have noted that the amount of the polymer that coprecipitates with the drug correlates with the ability of the polymer to maintain solution supersaturation.¹²

The purpose of this study is to further explore the impact of polymers on the crystallization tendency of highly supersaturated solutions containing amorphous drug nanodroplets, specifically exploring the relationship between crystallization and the amount of the polymer interacting with the drug-rich phase. To achieve this goal, the nucleation induction times for supersaturated solutions of enzalutamide were measured for solutions containing different amounts of colloidal drug species,

with varying amounts of polymers, focusing on hydroxypropyl methylcellulose acetate succinate (HPMCAS) and Eudragit E PO as examples of negatively and positively charged polymers, respectively, under intestinal pH conditions. Previous studies demonstrated that HPMCAS is an effective crystallization inhibitor for enzalutamide.¹³ The amount of HPMCAS or Eudragit E PO associated with the drug-rich nanodroplets versus the amount remaining in the aqueous solution was determined via nuclear magnetic resonance spectroscopy. Transmission electron microscopy (TEM) and fluorescence spectroscopy were used to further study the system. Molecular dynamics (MD) simulations were employed to provide insight into drug nanodroplet–polymer interactions.

EXPERIMENTAL SECTION

Drug and Polymer Structures. HPMCAS MF grade and Eudragit E PO were supplied by Shin-Etsu Co. Ltd (Tokyo, Japan) and Evonik (Essen, Germany), respectively. The novel cellulose derivative, CA-Pen079-HEA-3MPA¹⁴ (P177), was synthesized by the Edgar group as described previously.¹⁴ The molecular structures of these polymers, as well as that of the model drug, enzalutamide (ChemShuttle, Hayward, CA), are shown in Figure 1. Phenol, sulfuric acid, acid orange V, and chloroform were purchased from Fisher Scientific (Hampton, NH).

Dansylated HPMCAS Synthesis. Synthesis of dansylated 2-bromoethyl amine was achieved by slowly adding triethylamine (5.6 mL, 40 mmol) to a solution of dansyl chloride (5.0 g, 18.5 mmol) and 2-bromoethyl amine HBr (3.8 g, 18.5 mmol) in dimethylformamide (DMF) (60 mL). The resulting solution was stirred overnight and was then quenched with water. The product was extracted with EtOAc. The combined organic layers were washed with sat. aq NaHCO₃, followed by brine and were dried (MgSO₄). The crude product was purified by column chromatography (1:1 EtOAc/hexanes) to give 1.16 g of pure *N*-dansyl-2-bromoethyl amine (17% yield). ¹H NMR (300 MHz, CDCl₃): δ 8.2–8.8 (m, 3H), 7.2–7.7 (m, 3H), 5.9 (t, 1H), 3.6 (t, 2H), 3.3 (m, 2H), 2.9 (s, 6H).

Triethyl amine (8.6 mL, 62 mmol) was added to a solution of HPMCAS-MF (12 g) in DMF (70 mL). A solution of *N*-dansyl-2-bromoethyl amine (1.16 g, 3.1 mmol) in DMF (30 mL) was added, and the resulting solution was stirred for 3 days. The

reaction mixture was poured into water (1.5 L) with vigorous stirring. The solution was acidified with 10% aq HCl and then the precipitate was collected by filtration, washed with water, and dried to give 9.41 g of dansylated HPMCAS. The quantification of the amount of dansyl attached to HPMCAS is described in the [Supporting Information](#).

Characterization of Dansylated HPMCAS. ^1H and ^{13}C NMR were obtained using a Bruker ADVANCE II spectrometer at 500 MHz and were analyzed using CD_3CN and $\text{C}_5\text{D}_5\text{N}$. ^1H NMR samples were analyzed in 10 mg/mL solutions in CD_3CN (δ 1.94 ppm) or $\text{C}_5\text{D}_5\text{N}$ (δ 7.19, 7.55, and 8.71) with ^{13}C NMR in 50 mg/mL at 25 °C in 5 mm o.d. tubes with a minimum of 32 and 5000 number of scans, respectively. A full description of the analysis is provided in the [Supporting Information](#), Section S1.

Nucleation Induction Time Measurements. The previously described method to measure induction times was employed.¹⁵ In brief, the induction time, that is, the nucleation time plus the time needed to grow a detectable-sized crystal, was taken as the point where there was a decrease in absorbance at 237 nm, with a concurrent increase in the signal at a nonabsorbing wavelength of 446 nm. Representative spectra are shown in [Figure S2-1](#). Experiments were performed at varying initial concentrations of the model drug enzalutamide: 30, 35, 40, 45, 70, and 120 $\mu\text{g}/\text{mL}$, which represent concentrations below and above the concentration where nanodroplet formation occurs (GLPS, which is 42 $\mu\text{g}/\text{mL}$ for the experimental conditions employed). Based on the GLPS concentration of 42 $\mu\text{g}/\text{mL}$, the solutions prepared at an added concentration of 45, 70, and 120 $\mu\text{g}/\text{mL}$ contain 3, 28, and 78 $\mu\text{g}/\text{mL}$ of nanodroplets and 42 $\mu\text{g}/\text{mL}$ of molecularly dissolved enzalutamide. A stock solution of 10 mg/mL enzalutamide in methanol was aliquoted into 35 mL of 50 mM phosphate buffer, pH 6.5, containing a predissolved polymer. Eudragit E PO grade and HPMCAS MF grade were directly dissolved in the buffer, while P177 was predissolved in dimethyl sulfoxide followed by the addition of buffer such that the final concentration of the organic solvent was 1 ppm. The following concentrations of the polymer were tested: 30, 35, 40, 45, 70, and 120 $\mu\text{g}/\text{mL}$. The induction time experiments were performed in triplicate.

Nanodroplet Size and Surface Charge. The size and zeta potential of nanodroplets at varying concentration of enzalutamide and polymer were determined using dynamic light scattering (DLS) and zeta potential measurements, respectively. A 10 mg/mL stock solution of enzalutamide in methanol was added to a solution containing either P177, HPMCAS, or Eudragit E PO predissolved in pH 6.5 50 mM phosphate buffer to generate solutions containing different concentrations of the drug and polymer. Samples were stirred at 300 rpm at 37 °C for 5 min. Folded capillary zeta cells were used to measure zeta potential and particle size on a Nano-Zetasizer (Malvern Instruments, Westborough, MA) with dispersion technology software. The kinematic viscosity of solutions containing various concentrations of HPMCAS and Eudragit E PO solutions was determined at 37 °C using a Vibro viscometer SV-10 (A&D Ltd., Japan) and this value was input into the DLS instrument software to determine the hydrodynamic diameter of the particles. For all measurements, a refractive index of 1.33 was used and all samples had a PDI < 0.5. Experiments were performed in triplicate.

Polymer Distribution in Different Phases. *NMR Spectroscopy.* The distribution of HPMCAS and Eudragit between the bulk aqueous phase and the enzalutamide nanodroplets was determined by ^1H nuclear magnetic resonance (NMR)

spectroscopy, performed using a Bruker AVANCE-III-800 spectrometer (Billerica, MA) equipped with a QCI cryoprobe. The concentration of the polymer in the aqueous phase was directly measured from the NMR spectra, while the concentration of the polymer in the enzalutamide nanodroplets was determined by taking the difference between the total polymer concentration and the polymer concentration in the aqueous phase. The aqueous phase was a 50 mM pH 6.5 phosphate buffer consisting of 10% v/v deuterium oxide and 90% v/v water with 0.1 mg/mL trimethylsilylpropanoic acid used as a quantitative reference as well as a reference for the chemical shifts. An improved version of the WATERGATE method was used to suppress the signal from the water.^{16,17} The method was directly adopted from Ueda et al.¹⁸ HPMCAS and Eudragit solutions were prepared by adding 10, 25, 50, 100, and 200 $\mu\text{g}/\text{mL}$ of the respective polymer to the aqueous phase. These solutions were used to construct a linear standard curve for each polymer. For the HPMCAS solutions, the enzalutamide nanodroplet phase was generated by spiking 36 μL of enzalutamide stock solution, consisting of 10 mg/mL enzalutamide in $\text{DMSO}-d_6$, into 3 mL of solution to generate a total drug concentration of 120 $\mu\text{g}/\text{mL}$. For the Eudragit solutions, the enzalutamide nanodroplet phase was generated by spiking 21 μL of the enzalutamide stock solution into 3 mL of solution to generate a total drug concentration of 70 $\mu\text{g}/\text{mL}$. The solutions were pre-equilibrated to 37 °C and the spiking was carried out under constant stirring at 1000 rpm. The final solutions were stirred for either 15 min or 1 h and 15 min before 600 μL aliquots were collected in NMR tubes. The filled NMR tubes were equilibrated at 37 °C inside the AVANCE-III-800 spectrometer for approximately 3 min and were then scanned 16 times. The experiments were carried out in triplicate for each reported polymer concentration. The enzalutamide stock solution was also spiked into the aqueous phase without the polymer to determine the peak area of a select enzalutamide peak (2.69 ppm) corresponding to the maximum concentration of enzalutamide in the aqueous phase. The NMR spectra were analyzed using MestReNova version 14.1.0-24037 (Mestrelab Research S.L., Santiago de Compostela, Galicia, Spain). The strongest Eudragit peaks overlapped with enzalutamide and residual dimethyl sulfoxide (DMSO) peaks. Therefore, the Eudragit peaks in the region between 2.4 and 3.1 ppm were deconvoluted from the enzalutamide peak (2.98 ppm) and DMSO peak (2.69 ppm) using Global Spectral Deconvolution and were then integrated to obtain a sum area for the region. The HPMCAS peaks in the region between 2.8 and 4.2 ppm were also deconvoluted from the DMSO peak (2.69 ppm) using Global Spectral Deconvolution and were integrated to obtain a sum area for the region. Similarly, the spectra used for the standard curve had to be deconvoluted from the DMSO peak using the same method. The enzalutamide peak at 2.69 ppm was integrated after deconvolution to determine the amount of enzalutamide in the aqueous phase.

Fluorescence Spectroscopy. The fluorescence spectra of enzalutamide in the presence of dansylated HPMCAS (HPMCAS with a dansyl fluorophore attached) were used to evaluate the interaction of HPMCAS with the enzalutamide nanodroplets. Samples of enzalutamide with dansylated HPMCAS were analyzed on an RF-5301 PC spectrofluorophotometer Shimadzu (Kyoto, Japan). Enzalutamide (20–120 $\mu\text{g}/\text{mL}$) was added to dansylated HPMCAS (50 and 100 $\mu\text{g}/\text{mL}$) in buffer and subsequently vortexed for 5 s prior to measurements. The excitation wavelength was 380 nm with an excitation slit width of 5 nm and an emission slit width of 5 nm.

TEM Imaging. An FEI Tecnai G 20 electron microscope (FEI, Hillsboro, OR) equipped with a LaB6 source and operated at 200 keV was used to acquire bright-field (BF) transmission electron micrographs. Samples were prepared by pipetting an aliquot of the liquid sample onto 300 mesh ultrathin carbon-coated copper TEM grids with a thickness of 3–4 nm (SPI supplies, West Chester, PA) placed on a cellulose filter paper. The solution was allowed to cascade down the surface of the tilted grid as described previously.¹⁹ Liquid samples were evaluated at shorter and longer times than the nucleation induction times. Elemental analysis was performed to identify the drug and the polymer using an X-MAX silicon drift detector and energy-dispersive spectroscopy (EDX) detector (Oxford Instruments, Oxfordshire, UK). Fluorine was used as the distinguishing element since enzalutamide contains four fluorine atoms while the polymer do not contain fluorine. The beam spot size was chosen to be 4 to achieve the highest possible spatial resolution and a reasonable X-ray count rate. Image processing, including fast Fourier transform (FFT), was performed using Gatan Microscopy Suite Software. FFT processing was utilized herein to confirm the presence of crystalline enzalutamide. Three grids of each sample were tested.

MD Simulations of the Polymer with Enzalutamide.

Fully atomistic MD simulations were performed to provide insight into the interactions of a cluster of enzalutamide molecules with a polymer chain (Eud EPO and HPMCAS). The simulated systems included: (1) a 10-molecule enzalutamide aggregate in water, (2) the Eud EPO polymer chain and the HPMCAS polymer chain, and (3) the polymer chain in the presence of the drug aggregate in water. The total number of molecules (32,641) was maintained constant for all the simulations performed.

MD simulations were carried out in GROMACS 5.0,^{20,21} using the CHARMM force field.^{22,23}

Polymer Chain MD Simulations.

- (1) The polymer chains were sketched in HyperChem 8.0.3.²⁴ The Eud EPO polymer chain contained 12 units which consisted of 4 repetitions of three constant units (Figure 1b); the HPMCAS-MF polymer chain had 10 monomers with the composition shown in Table 1. The HPMCAS chain was simulated in an ionized state as would be expected at the experimental pH. The carboxylic acids in the three succinoyl functionalities were modeled as COO⁻.
- (2) An energy minimization of the polymer chain was performed, employing the BIO f (CHARMM) force field in HyperChem 8.0.3, with the Polak–Ribière

(conjugate gradient) algorithm, using a root-mean-square gradient of 1.0×10^{-2} kcal Å⁻¹ mol⁻¹ as the convergence condition. Then, the structures were submitted to the online topology building tool SwissParam²⁵ to obtain topology files in the GROMACS format for the CHARMM force field.

- (3) The polymers were solvated using the extended simple point charge (SPC/E) water model, with ~32,680 water molecules. In the case of HPMCAS, three Na⁺ ions were used as mobile counterions, in cubic boxes with edges of up to 10 nm. These ions served as counterions to the carboxylate groups of the HPMCAS polymer.
- (4) One minimization stage, two equilibration stages: an *NVT* and an *NPT*, and an *NPT* production run were performed. The leap-frog integrator and periodic boundary conditions with the Verlet cutoff scheme for neighbor searching were used. The particle mesh Ewald²⁶ method was used to model long-range electrostatics, whereas short-range electrostatics and van der Waals interactions were modeled with a cutoff of 1 nm. Energy groups for the drug, the polymer, the ions, and the solvent were specified in the MD simulation parameter file.
- (5) The minimization stage was performed with the steepest descent algorithm (0.01 fs/step), stopping when the maximum force was less than 100.0 kJ mol⁻¹ nm⁻¹. Then, an *NVT* equilibration was performed for 5 ns (1 fs/step) using the v-rescale thermostat, at a reference temperature of 310 K, with a coupling constant (τ -t) of 0.2 ps. Then, an *NPT* equilibration for 1 ns (1 fs/step) using the v-rescale thermostat, at a reference temperature of 310 K, with a coupling constant (τ -t) of 0.2 ps, and the Berendsen barostat at a reference pressure of 1 bar, with a coupling constant (τ -p) of 0.2 ps, were performed.
- (6) Finally, the production run was performed for 15 ns (1 fs/step recording output every 2 ps) in the isothermal–isobaric (*NPT*) ensemble using the Nosé–Hoover thermostat, at a reference temperature of 310 K, with a coupling constant (τ -t) of 0.2 ps; and the Parinello–Rahman barostat was performed at a reference pressure of 1 bar, with a coupling constant (τ -p) of 0.5 ps.

MD Simulation in the Gas Phase to Create an Enzalutamide Aggregate. The starting structure of enzalutamide was extracted from the crystal structure reported by Maini et al.²⁷ The drug structure was then submitted to the online topology building tool SwissParam to obtain the topology file. Ten drug molecules were added to a cubic box with edges of up to 10 nm. The system underwent a 0.5 ns *NVT* and a 2 ns *NPT* equilibration in the gas phase to create an aggregate of drug molecules.

Polymer–Drug MD Simulation. A similar procedure to the one reported in our previous publication was followed.²⁸ In brief, the enzalutamide aggregate was placed near the previously equilibrated polymer chain, separated by a distance of 1–2 nm. The combined system was solvated, and equilibration and production runs were performed using the same conditions described for single polymer chains in the previous section: 5 ns *NVT* and 1 ns *NPT* equilibrations followed by a 15 ns *NPT* production run. For the polymer–drug interaction analysis, the Lennard–Jones and Coulomb terms for short and 1–4 interactions were extracted. The GROMACS energy function was run for all energy groups along the production trajectory,

Table 1. Structural Information for the Polymer Chain Resembling the Composition of HPMCAS-MF^a

position	monomer									
	1	2	3	4	5	6	7	8	9	10
C2	H	H	M	H	H	H	H	H	M	H
C3	M	H	H	A	H	P	H	M	H	H
C6	H	S1	P	M	S2	M	A	S1	A	P

^aThe substituents are denoted as methoxyl (M), acetyl (A), hydroxypropoxyl (P), succinoyl (S1 = $-(C=O)CH_2CH_2COO^-$, S2 = $-CH_2CH(CH_3)O(C=O)CH_2CH_2COO^-$), and hydroxyl (H). There are three sites that can be substituted in each of the 10 monomers. Sites are denoted as C2, C3, and C6 according to their positions in the HPMCAS monomer.

with a flag to estimate the free energy difference with respect to an ideal gas state.²⁹

Statistical Analysis. Induction Time. Crystallization tendency for enzalutamide in the absence of the polymer above and below GLPS was assessed with a Kruskal–Wallis analysis of the variance test using OriginPro (OriginLab Corporation, Northampton, MA). Data were grouped into two groups: below GLPS and above GLPS.

Bayesian linear regression at a 95% confidence interval was performed in R³⁰ to assess the impact of drug concentration (below and above GLPS), polymer type, and polymer concentration on enzalutamide induction time. The regression model generates a formula for the log probability that a polymer will inhibit crystallization (with the assumption that crystallization was inhibited if no crystallization was observed after 720 min) based on four independent parameters: drug concentration, above and below GLPS, polymer type, and polymer concentration. For each independent parameter, it is assumed that the other independent parameters have no impact on it, that is, statistical findings for polymer type apply to all polymer and drug concentrations tested, statistical findings for above and below GLPS apply to all polymers, polymer concentrations tested, and so forth. Within the model, the base case scenario was arbitrarily identified by the program and is treated as the comparator for the groups within each independent variable. The base case situation was as follows: 30 $\mu\text{g}/\text{mL}$ enzalutamide for drug concentration, above GLPS for above/below GLPS, Eudragit for polymer type, and no polymer for polymer concentration.

The null hypothesis for each group within the independent variables was that the base case and test group come from the same population. At p values less than 0.05, the null hypothesis is rejected indicating that there is a statistically significant difference between the base case and the test group. The coefficient estimate indicates the probability of the test group crystallization will be inhibited as compared to the base case; positive estimate coefficients indicate that the test group has a higher probability of crystallization being inhibited as compared to the base case and vice versa for negative estimate coefficients. Results of these analyses are summarized in Tables S3-1 and S3-2.

Polymer Associated with Nanodroplets. The paired sample t -test was performed to assess the impact of the polymer and polymer concentration on the amount of the polymer associated with enzalutamide nanodroplets. For polymer concentration, the two groups were 50 and 100 $\mu\text{g}/\text{mL}$ (Table S3-3). To assess the impact of polymer type, 120 $\mu\text{g}/\text{mL}$ enzalutamide at 50 and 100 $\mu\text{g}/\text{mL}$ of HPMCAS and 70 $\mu\text{g}/\text{mL}$ were grouped together and compared to enzalutamide at 50 and 100 $\mu\text{g}/\text{mL}$ of Eudragit (Table S3-4).

RESULTS

In the absence of the polymer, enzalutamide crystallizes within 15 min both for supersaturated solutions that are free of nanodroplets, as well as from solutions containing nanodroplets (Figure 2). These induction times were divided into two groups: below GLPS, that is, under an enzalutamide concentration of 42 $\mu\text{g}/\text{mL}$ and above GLPS, that is, systems with an enzalutamide concentration above 42 $\mu\text{g}/\text{mL}$. Statistical analysis (Kruskal–Wallis test) at a 95% confidence interval was performed on the two groups; the null hypothesis was accepted indicating that there was no significant difference between induction times

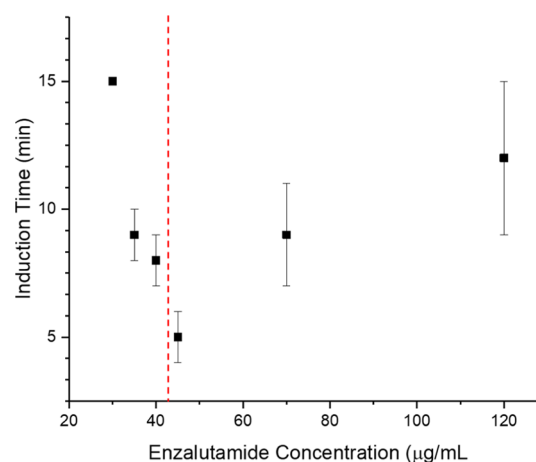


Figure 2. Induction time as a function of added enzalutamide concentration for concentrations above and below the GLPS concentration designated by the red dashed line (42 $\mu\text{g}/\text{mL}$). Data represent mean values \pm standard deviation for $n = 3$.

below and above GLPS in the absence of the polymer (see Table S3-1).

Figure 3 compares the impact of different concentrations of various polymers on the induction times of supersaturated solutions free of drug-rich nanodroplets (30–40 $\mu\text{g}/\text{mL}$) and those containing different amounts of nanodroplets (systems with added drug concentration greater than 42 $\mu\text{g}/\text{mL}$ initially contain nanodroplets prior to crystallization). It is apparent from Figure 3 that the effectiveness of the various polymers at preventing crystallization depends on polymer type, amount of the polymer present in the solution, and the initial concentration of the enzalutamide solutions and hence the amount of nanodroplets formed. The interdependence of these three factors can be more clearly seen from the summary 3D plot shown in Figure 4. The polymers extend the supersaturation duration by a few minutes or for several hours, depending on the system evaluated. From statistical analysis of the data (Table S3-2) and evaluation of the induction time data shown in Figures 3 and 4, several trends can be observed. First, it is clear that if all of the induction time data are considered, induction times are longer below the GLPS concentration than above the GLPS concentration. Second, Eudragit E PO is the least-effective polymer at inhibiting crystallization. From Table S3-2, it is not significantly different from the no polymer system when all drug concentrations are considered. From Figure 3b, a trend can be seen where Eudragit E PO is only effective at inhibiting crystallization at higher polymer concentrations and low drug concentrations. P177 is a significantly better crystallization inhibitor than Eudragit E PO and is particularly effective for enzalutamide solutions that do not contain nanodroplets. HPMCAS was more effective than the other polymers and at higher concentrations (≥ 50 $\mu\text{g}/\text{mL}$), could maintain supersaturation in enzalutamide systems containing a large amount of nanodroplets, as well as those without nanodroplets for several hours. In summary, these observations highlight that the effectiveness of a polymer as a crystallization inhibitor is dependent on its concentration and on the initial drug concentration and hence the amount of nanodroplets. It is more difficult for a polymer to delay crystallization when drug-rich nanodroplets are present. Therefore, when evaluating polymer effectiveness via nucleation induction time experiments, drug and polymer concentrations should be carefully

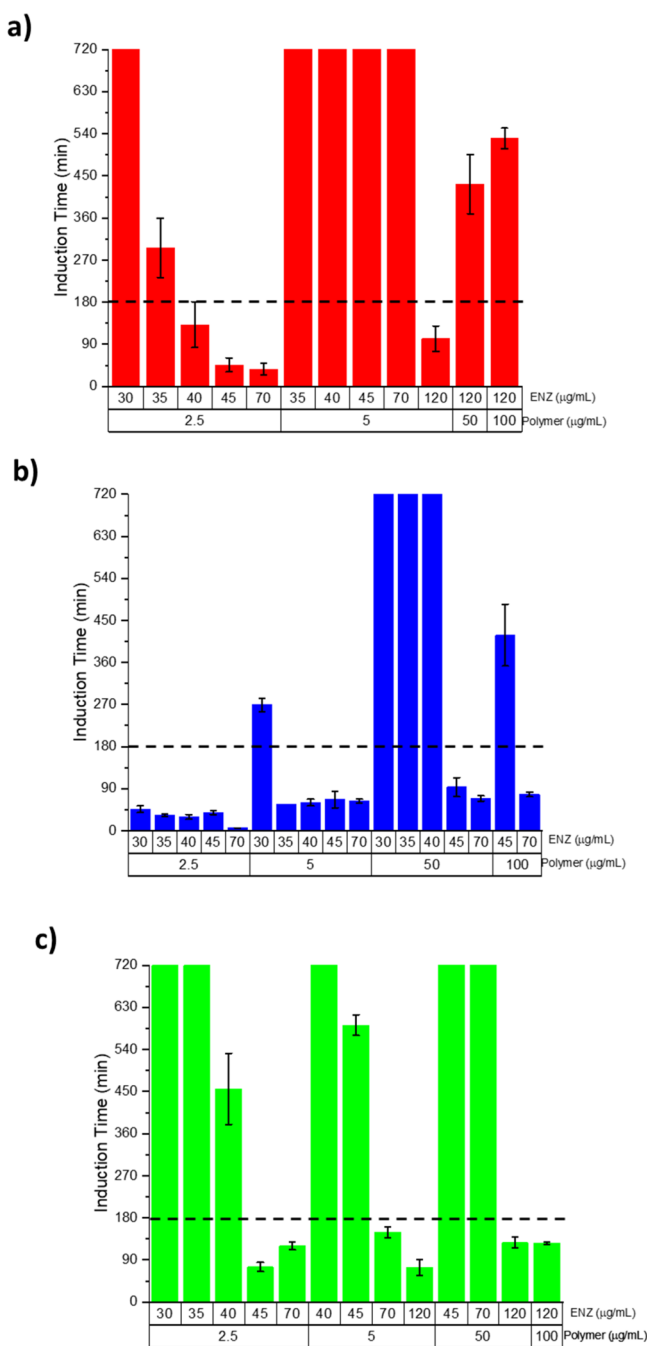


Figure 3. Induction time of enzalutamide solutions of varying initial concentrations in the presence of different amounts of (a) HPMCAS, (b) Eudragit E PO, and (c) P177. Values represent mean \pm standard deviation for $n = 3$. Bars without an error bar represent samples where no crystallization was observed by the end of the experiment (12 h) where $n = 3$. The dashed line represents the estimated biologically relevant timeframe for inhibition of crystallization (gastric residence and small intestine transit time of 180 min).

selected such that they resemble the concentrations generated when dissolving an ASD dosage form.

Given the differences observed between the polymers' effectiveness as crystallization inhibitors in the systems with and without drug-rich nanodroplets, the distribution of the polymer between the bulk aqueous phase and the drug-rich phase was assessed for Eudragit E PO and HPMCAS. Based on literature reports,^{11,12} the expectation was that the poor

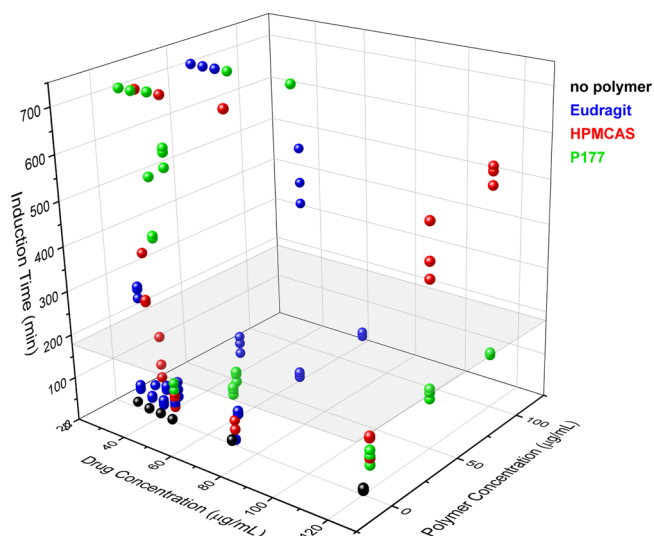


Figure 4. 3D plot summarizing all of the induction time data. Each point represents a single induction time experiment, where $n = 3$ for each condition tested. Drug concentration, polymer concentration, and polymer type were varied. Black data points are for drug alone, red are for HPMCAS, green are for P177, and blue are for Eudragit E PO. The horizontal plane provides an estimate of a biologically relevant timeframe for crystallization inhibition based on gastric residence and small intestine transit times (180 min).

inhibitory impact of Eudragit E PO in the presence of the drug-rich nanodroplets might arise because of a low concentration of the polymer associated with the nanodroplets.

Table 2 shows the amount of the polymer associated with the bulk aqueous solution and drug-rich nanodroplets, based on polymer depletion from solution as detected by ^1H NMR spectroscopy. It is apparent that a considerable amount of the polymer is associated with the drug-rich phase. Independent confirmation that the polymer was present in the drug-rich phase was obtained by pelleting the colloidal phase by centrifugation followed by colorimetric assay (see the Supporting Information and Table S4-1). For systems containing an initial Eudragit E PO concentration of 50–100 $\mu\text{g}/\text{mL}$, the resultant drug-rich nanodroplets contained approximately 40% w/w of the polymer. The amount of HPMCAS present in the nanodroplets increased as the initial concentration of HPMCAS in solution increased from 25 to 50 $\mu\text{g}/\text{mL}$ and for the highest HPMCAS concentration (100 $\mu\text{g}/\text{mL}$), the nanodroplets contained approximately 25% w/w polymer. No difference in polymer distribution was observed for an HPMCAS system mixed for 15 min compared to 75 min (Table 2), suggesting that equilibrium in polymer distribution between the bulk aqueous phase and the drug-rich nanodroplets was reached within 15 min. From Table 2 and statistical analysis (Table S3-4), it is apparent that Eudragit E PO distributed more into the drug-rich nanodroplets relative to HPMCAS for comparable polymer concentrations, although it should be noted that there were less drug-rich nanodroplets present in the Eudragit E PO system.

Given the amount of the polymer associated with the drug-rich phase, it was important to determine if the amorphous solubility was reduced. A second component that mixes substantially with the drug-rich phase would be expected to reduce the value of the amorphous solubility.^{31–35} Solution NMR is selective toward species dissolved in solution because species in a glassy state have low mobility and therefore the

Table 2. HPMCAS and Eudragit E PO Distribution in Enzalutamide Systems Containing Molecularly Dissolved Drug and Drug-Rich Nanodroplets after 1.25 h (HPMCAS) or 15 min (Eudragit) of Mixing^a

polymer	drug concentration ($\mu\text{g/mL}$)	polymer concentration ($\mu\text{g/mL}$)	polymer concentration in Solution ($\mu\text{g/mL}$)	w/w % polymer/ENZ nanodroplets
HPMCAS	120	25 ^b	12.6 (1.0)	12.7 (0.9)
	120	25	12.1 (2.0)	13.4 (1.9)
	120	50	28.4 (2.4)	19.3 (2.0)
	120	100	67.4 (3.0)	24.7 (1.9)
Eudragit	70	50 ^b	22.9 (1.0)	40.8 (0.8)
	70	100 ^b	67.9 (7.2)	41.0 (2.0)

^aValues in parentheses are standard deviations, $n = 3$. ^bReading taken after 15 min showing that polymer distribution occurs within this shorter timescale.

signals cannot be resolved using the instrument. Therefore, any depletion in enzalutamide solution concentration in the presence of the polymer can be determined from the intensity of enzalutamide solution peaks. Above the amorphous solubility, the enzalutamide concentration in solution is $42 \mu\text{g/mL}$. In the presence of both polymers, the bulk solution concentration of enzalutamide decreased with an increase in polymer concentration, with no differences apparent between the polymers, as shown in Figure 5.

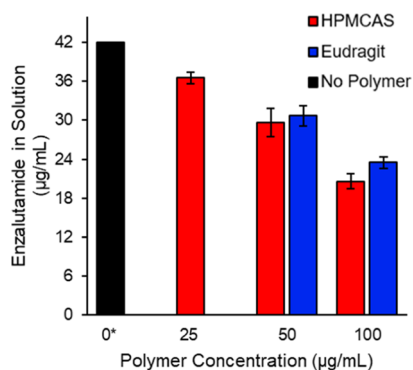


Figure 5. Enzalutamide concentration in solution in the presence and absence of the polymer. Samples with HPMCAS contained a total of $120 \mu\text{g/mL}$ of enzalutamide and samples with Eudragit contained a total of $70 \mu\text{g/mL}$ of enzalutamide. *Represents the amorphous solubility of enzalutamide (data not from NMR measurements).

To further investigate the polymer location, TEM imaging was performed. Transmission electron micrographs for HPMCAS and enzalutamide are shown in Figure 6. Approximately spherical enzalutamide droplets of diameter ranging from ~ 100 to 200 nm are present and surrounded by regions of the polymer. This was confirmed by the elemental composition of each of those regions using EDX. Fluorine (present in enzalutamide but not in the polymer) was used here to locate each component. The analyzed spherical nanospecies displayed $24 \pm 6\%$ fluorine demonstrating that they are drug-rich, while the surrounding regions displayed $4 \pm 2\%$ fluorine indicating that they are polymer-rich. Based on the image, HPMCAS appears to be associated with the drug-rich droplet perimeter. FFT of the droplets shown in Figure 6a (FFT image: Figure S5-1) did not exhibit any order, indicating that those droplets were amorphous.¹⁹ On the other hand, for samples that had undergone crystallization, the presence of lattice fringes could clearly be seen (Figure 6b) and the presence of crystalline enzalutamide was further confirmed using FFT analysis (Figure 6c³⁶). The FFT, in Figure 6c, indicates the presence of crystals in multiple orientations. It should be highlighted that the polymer

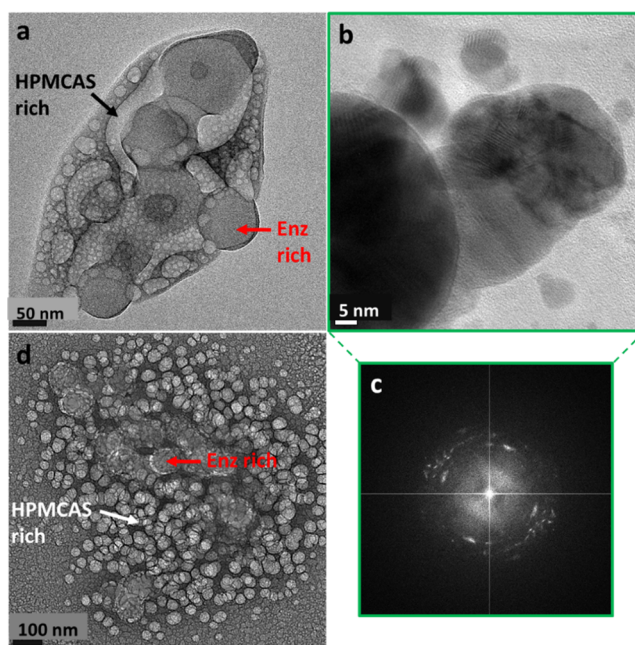


Figure 6. BF TE micrographs of (a) Enz ($120 \mu\text{g/mL}$):HPMCAS ($100 \mu\text{g/mL}$) nanodroplets, (b) Enz ($120 \mu\text{g/mL}$):HPMCAS ($100 \mu\text{g/mL}$) system after crystallization, (c) FFT of (b) confirming the presence of order due to crystallized Enz, and (d) Enz ($120 \mu\text{g/mL}$)-HPMCAS ($500 \mu\text{g/mL}$) showing both drug nanodroplets (larger spherical regions) and polymer aggregates (smaller, lighter spherical regions).

was not visible around the crystallized drug regions. For higher concentrations of HPMCAS, amorphous drug-rich droplets (100 – 150 nm) surrounded by smaller polymer aggregates of approximate size 20 – 50 nm are apparent (Figure 6d). In the case of the Eudragit E PO-enzalutamide system, the size range of the drug droplets is much larger, with agglomerates of the droplets being visible (Figure 7a). Again, the polymer appears to be associated with the periphery of the drug. Figure 7b shows an example of a crystalline agglomerate, displaying lattice fringes, confirmed by FFT analysis (Figure 7c,d).

The TEM images suggest that the polymer associates with the drug-rich nanodroplets at the drug–water interface. Therefore, it would be anticipated that the zeta potential would change in the presence of the polymer. This was found to be the case whereby the surface charge of nanodroplets varied with the polymer (Figure 8). In the absence of the polymer, the zeta potential was negative. When HPMCAS was present, the zeta potential became more negative, while with Eudragit E PO, the zeta potential was positive (Figure 8). These changes could be attributed to the polymer charge.^{37–39} HPMCAS is an anionic polymer while Eudragit E PO is a cationic polymer. Colloidal

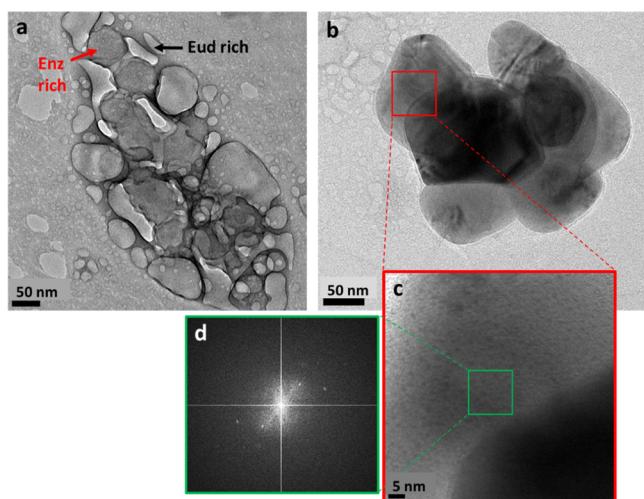


Figure 7. BF TE micrographs of (a) Enz (70 $\mu\text{g/mL}$):Eud (100 $\mu\text{g/mL}$) nanodroplets, (b) Enz crystals formed in the Eud solution, with zoomed-in region displaying order, and (d) FFT of (c) confirming the presence of order due to crystallized Enz. EDX analysis indicated that the spherical regions had $31.1 \pm 14\%$ fluorine indicating that they are drug-rich while the surrounding regions contained $6.3 \pm 5\%$ fluorine, indicating that they are mainly composed of the polymer.

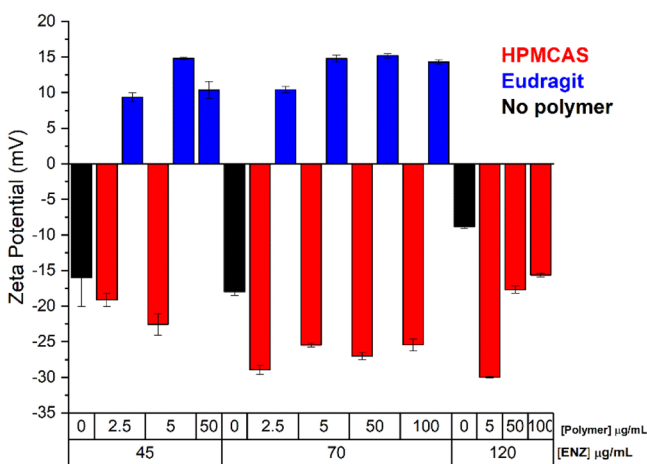


Figure 8. Zeta potential of enzalutamide nanodroplets in the presence of varying concentrations of the polymer.

species, such as drug-rich nanodroplets, can be sterically and electrostatically stabilized.³⁷ For colloidal species to be physically stable through electrostatic repulsion, the zeta potential of the colloidal species should be less than -30 mV or greater than $+30$ mV.^{40–42} If the surface charge is between -30 and $+30$ mV, the solution has the propensity to ripen over time.^{43–45} As most solutions tested had zeta potentials within this threshold, the most likely mechanism through which these polymers stabilize the nanodroplets is by sterically hindering the ripening of the nanospecies rather than through electrostatic repulsion.

The size of the colloidal species in the absence and presence of the polymer was also of interest, especially in terms of correlation to the TEM images, recognizing that DLS measures the hydrodynamic diameter. Polymer interaction with the droplet surface would be expected to impact the size measured, especially if droplet agglomeration is prevented. In samples prepared with the drug alone, the size of the drug-rich droplets increased rapidly with increasing drug concentration, most likely due to the agglomeration of the glassy droplets (Figure 9). The

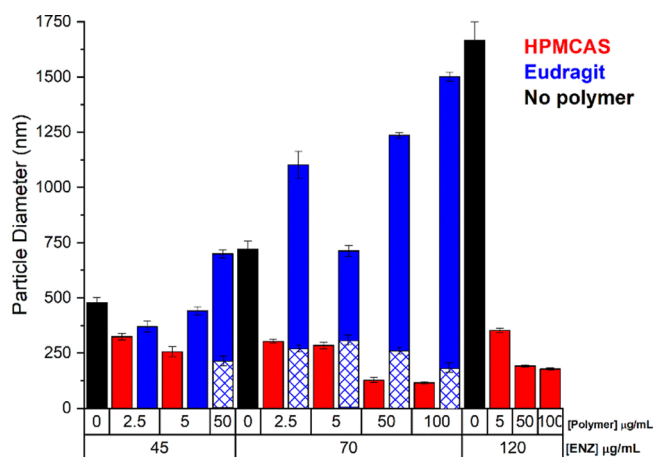


Figure 9. Initial diameter of the nanodroplets formed in the presence and absence of HPMCAS and Eudragit E PO. A bimodal distribution was observed for Eudragit E PO samples; different diameters for bimodal populations shown in solid color and hatched blue.

presence of the polymer impacted the hydrodynamic diameter of the colloidal species. With HPMCAS, the size of the colloidal species was 200–400 nm. For Eudragit E PO, the droplets ranged in size between approximately 200 and 1100 nm. Eudragit E PO was not tested above a drug concentration of 70 $\mu\text{g/mL}$ due to rapid drug crystallization. The smallest nanodroplets (80 nm) were observed for 70 $\mu\text{g/mL}$ enzalutamide and 50 $\mu\text{g/mL}$ HPMCAS. An approximately inverse relationship was observed for the size of nanodroplets and the concentration of Eudragit E PO in 70 $\mu\text{g/mL}$ enzalutamide. A reduction of nanodroplet size was only observed for higher polymer concentrations (50 and 100 $\mu\text{g/mL}$ Eudragit E PO) in 70 $\mu\text{g/mL}$ enzalutamide. However, in some systems, a bimodal size distribution was observed, suggesting that some agglomerates had formed (Supporting Information Section S6), consistent with the TEM images (Figure 7).

In order to better understand the interaction of polymers with the amorphous enzalutamide nanodroplets, HPMCAS, labeled with an environment-sensitive fluorescence tag, was utilized. The fluorescence emission spectrum of dansyl, which was used as the label, is highly dependent on the polarity of the local environment.⁴⁶ In a less polar environment, the fluorescence intensity increases, and the emission peak shifts to a lower wavelength, relative to a polar environment. To confirm that covalent linkage of dansyl to HPMCAS retained the probe environment sensitivity, the fluorescence emission spectra of the labeled polymer in buffer and dichloromethane were compared, with data being shown in Figure 10. A blue shift was observed for the dansylated HPMCAS (d-HPMCAS) spectrum in dichloromethane in comparison with the buffer, and the peak intensity increased. It was also determined that d-HPMCAS showed a similar effectiveness as a crystallization inhibitor as the nonlabeled polymer (data not shown), confirming that the polymer retained functionality as an inhibitor after labeling. Next, d-HPMCAS was added to solutions with different initial enzalutamide concentrations, containing various amounts of drug-rich nanodroplets. For enzalutamide solutions at a concentration below the amorphous solubility, both drug and polymer are molecularly dissolved and minimal interactions are anticipated between the solvated species. At concentrations above the amorphous solubility, enzalutamide will undergo

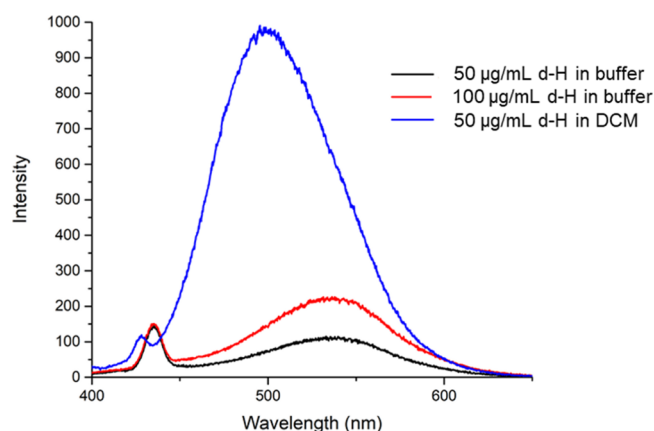


Figure 10. Fluorescence spectra of 50 and 100 $\mu\text{g/mL}$ dansylated HPMCAS (d-H) in buffer and dichloromethane (DCM).

GLPS with the formation of nanodroplets whereby this drug-rich phase is less polar than water. Hence, if d-HPMCAS associates with the nanodroplets, its emission characteristics are expected to change. In contrast, if there is no interaction, d-HPMCAS should have the same spectrum as in buffer or the low-concentration enzalutamide solutions. The fluorescence spectra of d-HPMCAS in buffer and enzalutamide solutions of different concentrations above and below the GLPS concentrations are shown in Figure 11. All spectra show a peak at approximately 437 nm, irrespective of the presence or absence of enzalutamide. In buffer without the drug, there is a broad, low intensity peak at around 535 nm which is present at around 528 nm at low enzalutamide concentrations. As the enzalutamide concentration increases beyond the amorphous solubility (42 $\mu\text{g/mL}$), new peaks emerge at 469 and 487 nm, and the emission peak has increased in intensity, whereby the overall maximum has shifted to a much lower wavelength, and the peak found at lower drug concentrations now presents as a shoulder at around 535 nm. This suggests that the dansylated portion of d-HPMCAS experiences two environments in the presence of the drug-rich nanodroplets, a less polar environment in which the polymer is interacting with the nanodroplets and a more polar aqueous environment. This is consistent with the results presented above that demonstrate that HPMCAS distributes between both phases. To check that dansylation did not impact the distribution of the polymer in terms of the amount associated with the nanodroplets versus the amount in bulk aqueous solution, the polymer concentration was assayed in each phase and was not found to be substantially different from that of the unlabeled polymer.

MD Simulations. MD simulations were used to provide a better understanding of the interaction between the ENZ nanodroplet and the polymers (HPMCAS or EUD E PO). The results from the MD simulations indicate that ENZ interacts with both polymers (Figure 12). Figure 13 shows the radial distribution functions (RDFs) between all the atoms of the polymer and all the atoms of the drug molecules; the similar curves observed for each polymer indicate that the distance between the polymer and drug is comparable in both cases. However, as can be seen from Figure 12, the polymers differ in their conformation; EUD E PO exhibits a globular structure, while HPMCAS has an extended conformation. The extended conformation for HPMCAS provides more surface to interact with the ENZ aggregate, explaining the more negative estimated free energy of interaction for ENZ-HPMCAS, as shown in

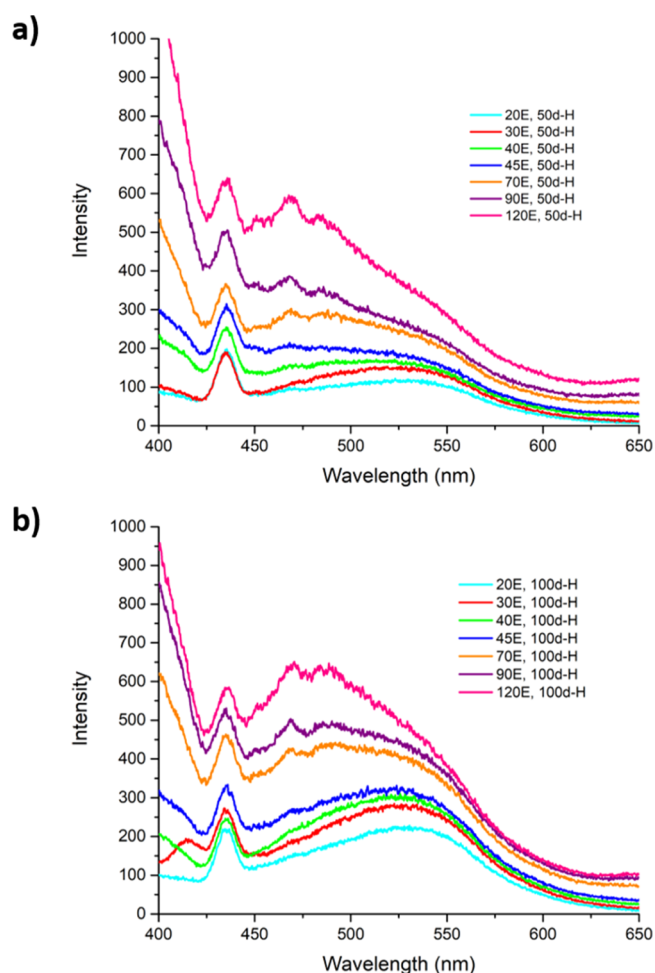


Figure 11. Fluorescence spectra of (a) 50 and (b) 100 $\mu\text{g/mL}$ solutions of dansylated HPMCAS (d-H) with varying concentrations of enzalutamide (E). The concentration where enzalutamide nanodroplets are expected to form is 42 $\mu\text{g/mL}$ of the drug.

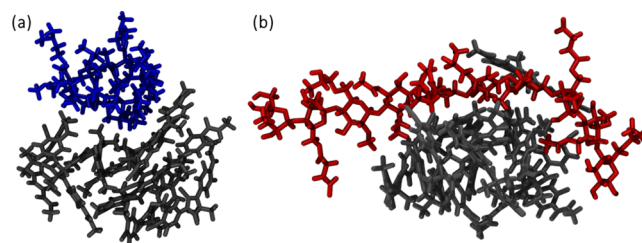


Figure 12. Representative snapshots from the 15 ns production trajectories of a nucleus of 10 molecules of enzalutamide (gray) and (a) Eud E PO in blue and (b) HPMCAS in red.

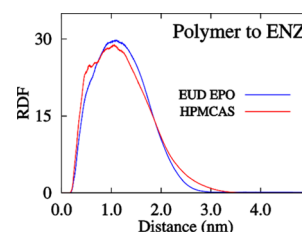


Figure 13. RDFs between the polymer and drug molecules, corresponding to the 15 ns trajectory.

Figure 14. Additional structural information, including radius of gyration, solvent-accessible surface area per atom, and estimated

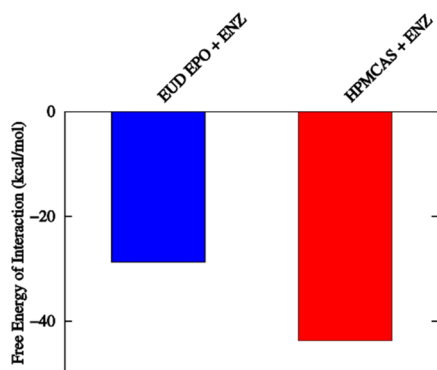


Figure 14. Estimated free energy of interaction for polymer–drug systems: Eud EPO and ENZ in blue and HPMCAS + ENZ in red.

drug–polymer interfacial area are shown in Figure S7-1 in the Supporting Information.

DISCUSSION

Amorphous drug-rich nanodroplets are frequently observed in aqueous solutions.³⁷ Of particular note, they form when the concentration of the drug in solution exceeds the amorphous solubility of the compound in a given medium.⁹ This suggests that solubility-enhancing formulations, designed to generate supersaturated solutions *in vivo*, are potentially prone to form nanodroplets following release of the drug from the formulation. To date, nanodroplet formation has been shown to occur *in vitro* following dissolution of certain ASDs, as a result of pH change,⁴⁷ following dissolution of a drug salt,⁴⁸ and following dilution of a concentrated organic solution of a drug.^{4,49} Drug-rich nanodroplets have also been found to form in an aspirated human intestinal fluid.⁵⁰ Because most drugs have melting points above room temperature, the amorphous form is metastable with respect to the crystal and there is thermodynamic driving force for crystallization. Hence, when nanodroplets form in solution, the solution remains supersaturated and crystallization is favored. Given that a metastable equilibrium exists between the drug present in the nanodroplet and the drug in the bulk aqueous solution, that is, the chemical potential of the drug in each phase is equivalent, there is an equal driving force for crystallization from each phase, although other factors important for crystallization, such as molecular mobility, vary between each phase. When the amorphous solubility is exceeded, either nanodroplet formation or crystallization is inevitable, whereby the formation and maintenance of nanodroplets are preferred over crystallization from a solubility enhancement and drug-delivery perspective, since nanodroplets coexist with a supersaturated bulk aqueous solution, while crystal formation results in a depletion of the supersaturation. It is widely recognized that supersaturated solutions show improved membrane transport and lead to a greater rate of permeation.^{51,52} Therefore, inhibiting crystallization in systems containing drug nanodroplets is desirable. However, the crystallization inhibition potential of a given polymer in the presence and absence of amorphous nanodroplets has not been extensively explored. Recent studies, both *in vitro* and *in vivo*, point to the advantageous properties of nanodroplet-containing systems.^{8,53,54} These studies suggest that the nanodroplets act as a depot, dissolving to replace drug absorbed across a membrane,

thereby maintaining supersaturation at a maximized value, driving membrane transport, and potentially enhancing absorption *in vivo*.^{4,6,7,55,56}

To maintain solution supersaturation, effective crystallization inhibitors that prevent drug crystallization from both the drug-rich phase and the bulk solution phase are necessary. This requires that the polymer associates with the drug present in each phase. This concept was discussed by Raina et al. in a study with felodipine where it was noted that the amount of the polymer associated with the nanodroplets appeared to correlate with the polymer hydrophobicity, for a given initial polymer concentration.¹⁰ Furthermore, it was found that polymers that had a high affinity for either the aqueous phase, or the drug-rich phase, were poor crystallization inhibitors. Therefore, it was suggested that a required criterion for an effective polymeric inhibitor in systems containing drug-rich nanodroplets is that the polymer distribute between both phases. Clearly, following distribution, the polymer must then inhibit crystallization in each phase. Ueda et al. studied several HPMC derivatives of differing hydrophobicities and also found that the amount of the polymer associated with the drug-rich nanodroplets increased with polymer hydrophobicity.¹¹ They further concluded that a greater extent of crystallization inhibition was observed for systems where there was more polymer associated with the drug-rich nanodroplets. Similar conclusions were drawn by Wang et al. when studying supersaturated solutions of posaconazole and HPMCAS, namely, that increased association of the polymer with the drug nanodroplets leads to supersaturation for a longer period of time.¹²

For the two polymers studied herein, we do not observe a link between the amount of the polymer associated with the drug-rich nanodroplets and the effectiveness of the polymer as a crystallization inhibitor. Eudragit E PO had greater association than HPMCAS with the drug-rich nanodroplets but was a less effective crystallization inhibitor. Hence, our results differ from the observations of Ueda et al. and Wang et al., namely, that crystallization inhibition correlates with the amount of the polymer associated with the droplet phase. By considering crystallization mechanisms, we can attempt to rationalize, at least to some extent, our observations. The first important consideration is that, in principle, crystallization can occur from either phase. Therefore, an effective polymer must be able to prevent crystallization from the bulk solution phase. This can be evaluated by studying crystallization from droplet-free solutions, that is, those at a concentration below the amorphous solubility. We note that in the absence of nanodroplets, Eudragit E PO is an effective inhibitor of solution crystallization when present at a concentration of 50 $\mu\text{g/mL}$, as is HPMCAS (Figure 3). However, Eudragit E PO is not an effective inhibitor when drug nanodroplets are present. Consequently, the relatively poor performance of Eudragit E PO compared to HPMCAS in the presence of nanodroplets appears to be related to the ability of each polymer to inhibit crystallization from the droplet phase or at the interface between the droplet phase and the bulk solution. One possible explanation is that substantial mixing of the polymer with the drug droplet phase reduces the drug chemical potential, and hence the driving force for crystallization, and that this occurs to a different extent for each polymer. The amorphous solubility, which depends on the chemical potential of the drug in the droplet phase, would be reduced in the presence of the polymer, with the extent of the reduction depending on the amount of the polymer mixed with the drug and any mixing nonidealities. Such reductions in amorphous

solubility by polymer mixing with the drug-rich nanodroplet have been observed previously for some systems.^{57,58} We note from Figure 5 that mixing of the polymers with the drug-rich nanodroplet does indeed reduce the drug amorphous solubility. However, there was no difference in the extent of reduction between the two polymers. Since no detectable difference in the amorphous solubility of enzalutamide in the presence of either polymer was observed, this suggests that the thermodynamic driving force for crystallization is similar and that other factors need to be considered to explain the difference in polymer crystallization inhibition effectiveness.

The interaction of each polymer with the droplet surface is supported by the zeta potential data (Figure 8), the TEM images (Figures 6 and 7), and the MD simulations (Figure 12). It is widely accepted that heterogeneous nucleation reduces the barrier for nucleation, and hence, nucleation at an interface typically proceeds more readily than nucleation in the absence of a suitable surface.⁵⁹ The interface of the drug-rich droplet with the solvent is likely a highly favorable site for heterogeneous nucleation. Altering the surface chemistry of an interface via additives can be expected to enhance or retard nucleation, depending on how the additive interacts with the interface.⁶⁰ Our results demonstrate that in the presence of polymers, it is much harder to inhibit crystallization in systems containing droplets, relative to that in nanodroplet-free supersaturated solutions, with induction times trending faster as the number of droplets increases (Figures 3 and 4). This observation supports the conjecture that the presence of drug-rich droplets is favorable for crystallization. It should be noted that the supersaturation does not increase once the amorphous solubility is exceeded; once the amorphous solubility is reached, excess drug above this concentration forms a new phase (the drug-rich droplets), and the chemical potential of the drug in each phase remains constant and equivalent. However, several systems showed a marked decrease in induction time when the concentration increases from just below the amorphous solubility (e.g., induction times at 40 $\mu\text{g}/\text{mL}$ which is just below the amorphous solubility of 42 $\mu\text{g}/\text{mL}$) to just above the amorphous solubility (e.g., induction times at 45 $\mu\text{g}/\text{mL}$), as shown in Figures 3 and 4. Further decreases in induction time are apparent as the number of droplets is increased and higher amounts of the polymer are required to delay crystallization. Therefore, the droplets tend to enhance the crystallization tendency of the system, and crystallization inhibition of this phase is essential. It is also important to consider the induction time data (summarized in Figure 4) in the context of biologically relevant timeframes for crystallization. Given that most drugs are predominantly absorbed in the small intestine, we can approximate a biologically relevant timeframe as being related to the gastric residence time and/or the small intestinal transit time. For acidic polymers, where polymer dissolution and drug release only occur at higher pH values, only the small intestinal transit time is likely relevant, while for polymers soluble at low pH, for example, Eudragit E PO, the gastric residence time is also important. In Figure 4, an estimation of gastric residence and small intestinal transit times (based on mean values of 1 and 3 h, respectively)⁶¹ shows that enzalutamide systems below the GLPS concentration tend to remain supersaturated for relevant time periods, as long as sufficient polymer is present. Above the GLPS concentration, only HPMCAS is effective at maintaining supersaturation over the required time period.

The cellulose derivatives, P177 and HPMCAS, which are anionic at the pH tested, were effective crystallization inhibitors

at concentrations above and below the amorphous solubility. HPMCAS has been shown to be effective at maintaining supersaturation for multiple structurally diverse, poorly water-soluble compounds.^{6,62–68} The effectiveness of HPMCAS has been attributed to the presence of hydrophobic regions that can interact with nonpolar regions of the drug in aqueous solution, as well as the presence of a charge arising from carboxylic acid groups that ionize at pH values above 5–6, which interact with water, allowing the polymer to be solvated.^{63,64,69} Overall, these chemical features lead to amphiphilic properties and it has been demonstrated that HPMCAS adsorbs at the drug crystal/water interface with a more extended conformation when ionized versus when partially ionized.⁷⁰ These molecular features should also drive interaction with the drug-rich nanodroplets, and results with fluorescently labeled HPMCAS (Figure 11) confirm close interaction of the polymer with enzalutamide droplets. Considering these chemical features, it might be anticipated that Eudragit E PO would exhibit a similar behavior to HPMCAS since it is an amino methacrylate copolymer and thus contains both hydrophobic moieties and the cationic amino group which is ionized at pH 6.5. This polymer does indeed interact with enzalutamide nanodroplets, with a greater amount associated with the nanodroplets than for HPMCAS. However, despite both polymers associating with the nanodroplets, Eudragit E PO was far less effective at inhibiting enzalutamide crystallization than HPMCAS in solutions containing nanodroplets. The MD simulations show insight into possible reasons underlying the different crystallization inhibition properties. Thus, although both polymers were found to associate with the ENZ aggregates in the MD simulations, the extent of interaction varied. EPO has a globular structure, limiting its interaction with the ENZ aggregate, while HPMCAS has an extended structure that allows a larger surface area of interaction. This agrees with our previous observations showing that polymers that exhibit strong intramolecular interactions in water, favoring globular conformations, tend to be less-effective crystallization inhibitors than those polymers with an extended conformation.^{15,28} Furthermore, Liu et al. have pointed out that additives adsorbed to the surface of a nucleus need to be desorbed, for solute molecules to be incorporated into the embryo.⁷¹ Thus, there is a desolvation energy barrier to be overcome. Based on the interaction-estimated free energies (Figure 14), this energy barrier is expected to be larger for HPMCAS, consistent with its greater effectiveness as an inhibitor.

CONCLUSIONS

In the absence of inhibitory additives, enzalutamide crystallized rapidly from supersaturated solutions. Both anionic and cationic polymers, specifically HPMCAS and Eudragit E PO, were effective crystallization inhibitors in homogeneous, single-phase supersaturated solutions, that is, solutions at a concentration below the amorphous solubility. When drug-rich nanodroplets were formed, the polymers became less effective at maintaining supersaturation, and a greater polymer concentration was required to extend induction times. Analysis of the amount of each polymer associated with the drug-rich nanodroplets demonstrated that Eudragit E PO had a higher tendency to incorporate into the nanodroplets. However, HPMCAS more effectively stabilized the drug-rich nanodroplets against both crystallization and size enlargement. The stabilization against crystallization in supersaturated aqueous solutions containing enzalutamide nanodroplets may be mediated by interactions between the drug and the polymer at the nanodroplet/water

interface. MD simulations revealed that the polymer conformation at the nanodroplet/water interface may be critical in explaining the observed differences. Thus, we propose that to achieve inhibition of crystallization in solutions containing drug-rich nanodroplets, the polymer must first distribute between the aqueous and drug-rich phase and second must adopt a certain conformation at the nanodroplet/water interface to effectively prevent the formation and/or growth of embryonic crystals. Additional mechanisms may also be important, and further studies are clearly warranted.

■ ASSOCIATED CONTENT

Supporting Information

The Supporting Information is available free of charge at <https://pubs.acs.org/doi/10.1021/acs.molpharmaceut.0c00833>.

Quantification of the amount of dansyl attached to HPMCAS; example UV spectra; statistical analysis; colorimetric polymer analysis; TEM image of enzalutamide nanodroplets showing the FFT pattern; DLS size distribution data for enzalutamide nanodroplets; and additional information from MD simulations: radius of gyration, solvent-accessible surface area per atom, and estimated drug–polymer interfacial area (PDF)

■ AUTHOR INFORMATION

Corresponding Author

Lynne S. Taylor – Department of Industrial & Physical Pharmacy, College of Pharmacy, Purdue University, West Lafayette, Indiana 47907, United States; orcid.org/0000-0002-4568-6021; Email: lstaylor@purdue.edu

Authors

Venecia R. Wilson – Department of Industrial & Physical Pharmacy, College of Pharmacy, Purdue University, West Lafayette, Indiana 47907, United States

Naila A. Mugheirbi – Department of Industrial & Physical Pharmacy, College of Pharmacy, Purdue University, West Lafayette, Indiana 47907, United States

Laura I. Mosquera-Giraldo – Department of Industrial & Physical Pharmacy, College of Pharmacy, Purdue University, West Lafayette, Indiana 47907, United States; orcid.org/0000-0003-4045-5491

Alexandru Deac – Department of Industrial & Physical Pharmacy, College of Pharmacy, Purdue University, West Lafayette, Indiana 47907, United States

Dana E. Moseson – Department of Industrial & Physical Pharmacy, College of Pharmacy, Purdue University, West Lafayette, Indiana 47907, United States; orcid.org/0000-0001-6986-8252

Daniel T. Smith – Department of Industrial & Physical Pharmacy, College of Pharmacy, Purdue University, West Lafayette, Indiana 47907, United States

Diana C. Novo – Department of Chemistry, College of Science, Virginia Tech, Blacksburg, Virginia 24061, United States; orcid.org/0000-0002-8317-4801

Carlos H. Borca – Department of Chemical and Biological Engineering, School of Engineering and Applied Science, Princeton University, Princeton, New Jersey 08544, United States; orcid.org/0000-0003-0683-7613

Lyudmila V. Slipchenko – Department of Chemistry, College of Science, Purdue University, West Lafayette, Indiana 47907, United States

Kevin J. Edgar – Department of Chemistry, College of Science, Virginia Tech, Blacksburg, Virginia 24061, United States; orcid.org/0000-0002-9459-9477

Complete contact information is available at: <https://pubs.acs.org/doi/10.1021/acs.molpharmaceut.0c00833>

Notes

The authors declare no competing financial interest.

■ ACKNOWLEDGMENTS

Gratitude is extended to PhRMA Foundation for providing financial support to conduct this research via a Pre-Doctoral Fellowship awarded to V.R.W. This research was supported in part by a Graduate Student Fellowship Award from the American Association of Pharmaceutical Scientists (AAPS) to L.I.M.-G. We also express thanks for funding provided by the McKeehan Graduate Fellowship in Pharmacy and the Migliaccio/Pfizer Graduate Fellowship in Pharmaceutical Sciences awarded to L.I.M.-G. We would like to acknowledge the National Science Foundation for their financial support through grant DMR-1309218. This research was supported in part through computational resources provided by Information Technology at Purdue University. Finally, we would like to acknowledge Ashish and Prof. Arman Sabbaghi at Purdue University Statistical Consulting Services for performing statistical analysis on data.

■ REFERENCES

- (1) Benet, L. Z. The Role of BCS (Biopharmaceutics Classification System) and BDDCS (Biopharmaceutics Drug Disposition Classification System) in Drug Development. *J. Pharm. Sci.* **2013**, *102*, 34–42.
- (2) Baghel, S.; Cathcart, H.; O'Reilly, N. J. Polymeric Amorphous Solid Dispersions: A Review of Amorphization, Crystallization, Stabilization, Solid-State Characterization, and Aqueous Solubilization of Biopharmaceutical Classification System Class II Drugs. *J. Pharm. Sci.* **2016**, *105*, 2527–2544.
- (3) Dahan, A.; Miller, J. M. The Solubility-Permeability Interplay and Its Implications in Formulation Design and Development for Poorly Soluble Drugs. *AAPS J.* **2012**, *14*, 244–251.
- (4) Mosquera-Giraldo, L. I.; Taylor, L. S. Glass–Liquid Phase Separation in Highly Supersaturated Aqueous Solutions of Telaprevir. *Mol. Pharm.* **2015**, *12*, 496–503.
- (5) Indulkar, A. S.; Waters, J. E.; Mo, H.; Gao, Y.; Raina, S. A.; Zhang, G. G. Z.; Taylor, L. S. Origin of Nanodroplet Formation Upon Dissolution of an Amorphous Solid Dispersion: A Mechanistic Isotope Scrambling Study. *J. Pharm. Sci.* **2017**, *106*, 1998–2008.
- (6) Raina, S. A.; Zhang, G. G. Z.; Alonzo, D. E.; Wu, J.; Zhu, D.; Catron, N. D.; Gao, Y.; Taylor, L. S. Enhancements and Limits in Drug Membrane Transport Using Supersaturated Solutions of Poorly Water Soluble Drugs. *J. Pharm. Sci.* **2014**, *103*, 2736–2748.
- (7) Indulkar, A. S.; Gao, Y.; Raina, S. A.; Zhang, G. G. Z.; Taylor, L. S. Exploiting the Phenomenon of Liquid-Liquid Phase Separation for Enhanced and Sustained Membrane Transport of a Poorly Water-Soluble Drug. *Mol. Pharm.* **2016**, *13*, 2059–2069.
- (8) Wilson, V.; Lou, X.; Osterling, D. J.; Stolarik, D. F.; Jenkins, G.; Gao, W.; Zhang, G. G. Z.; Taylor, L. S. Relationship between Amorphous Solid Dispersion In Vivo Absorption and In Vitro Dissolution: Phase Behavior during Dissolution, Speciation, and Membrane Mass Transport. *J. Controlled Release* **2018**, *292*, 172–182.

- (9) Taylor, L. S.; Zhang, G. G. Z. Physical Chemistry of Supersaturated Solutions and Implications for Oral Absorption. *Adv. Drug Delivery Rev.* **2016**, *101*, 122–142.
- (10) Raina, S. A.; Van Eerdenbrugh, B.; Alonzo, D. E.; Mo, H.; Zhang, G. G. Z.; Gao, Y.; Taylor, L. S. Trends in the Precipitation and Crystallization Behavior of Supersaturated Aqueous Solutions of Poorly Water-Soluble Drugs Assessed Using Synchrotron Radiation. *J. Pharm. Sci.* **2015**, *104*, 1981–1992.
- (11) Ueda, K.; Higashi, K.; Yamamoto, K.; Moribe, K. Inhibitory Effect of Hydroxypropyl Methylcellulose Acetate Succinate on Drug Recrystallization from a Supersaturated Solution Assessed Using Nuclear Magnetic Resonance Measurements. *Mol. Pharm.* **2013**, *10*, 3801–3811.
- (12) Wang, S.; Liu, C.; Chen, Y.; Zhu, A.; Qian, F. Aggregation of Hydroxypropyl Methylcellulose Acetate Succinate under Its Dissolving PH and the Impact on Drug Supersaturation. *Mol. Pharm.* **2018**, *15*, 4643–4653.
- (13) Wilson, V. R.; Lou, X.; Osterling, D. J.; Stolarik, D. F.; Jenkins, G. J.; Nichols, B. L. B.; Dong, Y.; Edgar, K. J.; Zhang, G. G. Z.; Taylor, L. S. Amorphous Solid Dispersions of Enzalutamide and Novel Polysaccharide Derivatives: Investigation of Relationships between Polymer Structure and Performance. *Sci. Rep.* **2020**, *10*, 18535.
- (14) Meng, X.; Roy Choudhury, S.; Edgar, K. J. Multifunctional Cellulose Esters by Olefin Cross-Metathesis and Thiol-Michael Addition. *Polym. Chem.* **2016**, *7*, 3848–3856.
- (15) Mosquera-Giraldo, L. I.; Borca, C. H.; Meng, X.; Edgar, K. J.; Slipchenko, L. V.; Taylor, L. S. Mechanistic Design of Chemically Diverse Polymers with Applications in Oral Drug Delivery. *Biomacromolecules* **2016**, *17*, 3659–3671.
- (16) Piotta, M.; Saudek, V.; Sklenář, V. Gradient-Tailored Excitation for Single-Quantum NMR Spectroscopy of Aqueous Solutions. *J. Biomol. NMR* **1992**, *2*, 661–665.
- (17) Liu, M.; Mao, X.-a.; Ye, C.; Huang, H.; Nicholson, J. K.; Lindon, J. C. Improved Watergate Pulse Sequences for Solvent Suppression in NMR Spectroscopy. *J. Magn. Reson.* **1998**, *132*, 125–129.
- (18) Ueda, K.; Hate, S. S.; Taylor, L. S. Impact of Hypromellose Acetate Succinate Grade on Drug Amorphous Solubility and In Vitro Membrane Transport. *J. Pharm. Sci.* **2020**, *109*, 2464–2473.
- (19) Mugheirbi, N. A.; Marsac, P. J.; Taylor, L. S. Insights into Water-Induced Phase Separation in Itraconazole-Hydroxypropylmethyl Cellulose Spin Coated and Spray Dried Dispersions. *Mol. Pharm.* **2017**, *14*, 4387–4402.
- (20) Van Der Spoel, D.; Lindahl, E.; Hess, B.; Groenhof, G.; Mark, A. E.; Berendsen, H. J. C. GROMACS: Fast, Flexible, and Free. *J. Comput. Chem.* **2005**, *26*, 1701–1718.
- (21) Hess, B.; Kutzner, C.; Van Der Spoel, D.; Lindahl, E. GROMACS 4: Algorithms for Highly Efficient, Load-Balanced, and Scalable Molecular Simulation. *J. Chem. Theory Comput.* **2008**, *4*, 435–447.
- (22) Brooks, B. R.; Bruccoleri, R. E.; Olafson, B. D.; States, D. J.; Swaminathan, S.; Karplus, M. CHARMM: A Program for Macromolecular Energy, Minimization, and Dynamics Calculations. *J. Comput. Chem.* **1983**, *4*, 187–217.
- (23) MacKerell, A. D.; Banavali, N.; Foloppe, N. Development and Current Status of the CHARMM Force Field for Nucleic Acids. *Biopolymers* **2000**, *56*, 257–265.
- (24) Froimowitz, M. HyperChem(TM): A Software Package for Computational Chemistry and Molecular Modeling. *Biotechniques* **1993**, *14*, 1010–1013.
- (25) Zoete, V.; Cuendet, M. A.; Grosdidier, A.; Michielin, O. SwissParam: A Fast Force Field Generation Tool for Small Organic Molecules. *J. Comput. Chem.* **2011**, *32*, 2359–2368.
- (26) Essmann, U.; Perera, L.; Berkowitz, M. L.; Darden, T.; Lee, H.; Pedersen, L. G. A Smooth Particle Mesh Ewald Method. *J. Chem. Phys.* **1995**, *103*, 8577–8593.
- (27) Maini, L.; Braga, D.; Farinella, F.; Melotto, E.; Verzini, M.; Brescello, R.; Michieletto, I.; Munari, I. Crystal Forms of Enzalutamide and a Crystal Engineering Route to Drug Purification. *Cryst. Growth Des.* **2018**, *18*, 3774–3780.
- (28) Mosquera-Giraldo, L. I.; Borca, C. H.; Parker, A. S.; Dong, Y.; Edgar, K. J.; Beaudoin, S. P.; Slipchenko, L. V.; Taylor, L. S. Crystallization Inhibition Properties of Cellulose Esters and Ethers for a Group of Chemically Diverse Drugs: Experimental and Computational Insight. *Biomacromolecules* **2018**, *19*, 4593–4606.
- (29) Abraham, M.; Hess, B.; van der Spoel, D.; Lindahl, E. *GROMACS Reference Manual*, 2018.
- (30) Core Team, R. R. *A Language and Environment for Statistical Computing*; R Foundation for Statistical Computing: Vienna, Austria, 2018.
- (31) Trasi, N. S.; Taylor, L. S. Dissolution Performance of Binary Amorphous Drug Combinations - Impact of a Second Drug on the Maximum Achievable Supersaturation. *Int. J. Pharm.* **2015**, *496*, 282–290.
- (32) Trasi, N. S.; Taylor, L. S. Thermodynamics of Highly Supersaturated Aqueous Solutions of Poorly Water-Soluble Drugs - Impact of a Second Drug on the Solution Phase Behavior and Implications for Combination Products. *J. Pharm. Sci.* **2015**, *104*, 2583–2593.
- (33) Li, N.; Taylor, L. S. Tailoring Supersaturation from Amorphous Solid Dispersions. *J. Controlled Release* **2018**, *279*, 114–125.
- (34) Lindfors, L.; Skantze, P.; Skantze, U.; Rasmusson, M.; Zackrisson, A.; Olsson, U. Amorphous Drug Nanosuspensions. 1. Inhibition of Ostwald Ripening. *Langmuir* **2006**, *22*, 906–910.
- (35) Lindfors, L.; Forssén, S.; Skantze, P.; Skantze, U.; Zackrisson, A.; Olsson, U. Amorphous Drug Nanosuspensions. 2. Experimental Determination of Bulk Monomer Concentrations. *Langmuir* **2006**, *22*, 911.
- (36) Moseson, D. E.; Taylor, L. S. The Application of Temperature-Composition Phase Diagrams for Hot Melt Extrusion Processing of Amorphous Solid Dispersions to Prevent Residual Crystallinity. *Int. J. Pharm.* **2018**, *553*, 454–466.
- (37) Ganesh, A. N.; Donders, E. N.; Shoichet, B. K.; Shoichet, M. S. Colloidal Aggregation: From Screening Nuisance to Formulation Nuisance. *Nano Today* **2018**, *19*, 188–200.
- (38) Li, J.; Lee, I. W.; Shin, G. H.; Chen, X.; Park, H. J. Curcumin-Eudragit e PO Solid Dispersion: A Simple and Potent Method to Solve the Problems of Curcumin. *Eur. J. Pharm. Biopharm.* **2015**, *94*, 322–332.
- (39) Marks, J. A.; Wegiel, L. A.; Taylor, L. S.; Edgar, K. J. Pairwise Polymer Blends for Oral Drug Delivery. *J. Pharm. Sci.* **2014**, *103*, 2871–2883.
- (40) Müller, R. H.; Hildebrand, G. E.; Nitzsche, R.; Paulke, B.-R. *Zetapotential Und Partikelladung in Der Laborpraxis*; Paperback APV; Wissenschaftliche Verlagsgesellschaft, 1996; Vol. 37.
- (41) Riddick, T. M. *Zeta-Meter Manual*; Zeta-Meter Inc.: New York, 1968.
- (42) Jacobs, C.; Müller, R. H. Production and Characterization of a Budesonide Nanosuspension for Pulmonary Administration. *Pharm. Res.* **2002**, *19*, 189–194.
- (43) Mugheirbi, N. A.; Tajber, L. Mesophase and Size Manipulation of Itraconazole Liquid Crystalline Nanoparticles Produced via Quasi Nanoemulsion Precipitation. *Eur. J. Pharm. Biopharm.* **2015**, *96*, 226–236.
- (44) Studart, A. R.; Amstad, E.; Gauckler, L. J. Colloidal Stabilization of Nanoparticles in Concentrated Suspensions. *Langmuir* **2007**, *23*, 1081–1090.
- (45) Vandervoort, J.; Ludwig, A. Biocompatible Stabilizers in the Preparation of PLGA Nanoparticles: A Factorial Design Study. *Int. J. Pharm.* **2002**, *238*, 77–92.
- (46) Ren, B.; Gao, F.; Tong, Z.; Yan, Y. Solvent Polarity Scale on the Fluorescence Spectra of a Dansyl Monomer Copolymerizable in Aqueous Media. *Chem. Phys. Lett.* **1999**, *307*, 55–61.
- (47) Indulkar, A. S.; Box, K. J.; Taylor, R.; Ruiz, R.; Taylor, L. S. PH-Dependent Liquid-Liquid Phase Separation of Highly Supersaturated Solutions of Weakly Basic Drugs. *Mol. Pharm.* **2015**, *12*, 2365–2377.
- (48) Almeida E Sousa, L.; Reutzel-Edens, S. M.; Stephenson, G. A.; Taylor, L. S. Supersaturation Potential of Salt, Co-Crystal, and

Amorphous Forms of a Model Weak Base. *Cryst. Growth Des.* **2016**, *16*, 737–748.

(49) Ilevbare, G. A.; Taylor, L. S. Liquid–Liquid Phase Separation in Highly Supersaturated Aqueous Solutions of Poorly Water-Soluble Drugs: Implications for Solubility Enhancing Formulations. *Cryst. Growth Des.* **2013**, *13*, 1497–1509.

(50) Elkhazab, A.; Moseson, D. E.; Brouwers, J.; Augustijns, P.; Taylor, L. S. Interplay of Supersaturation and Solubilization: Lack of Correlation between Concentration-Based Supersaturation Measurements and Membrane Transport Rates in Simulated and Aspirated Human Fluids. *Mol. Pharm.* **2019**, *16*, 5042–5053.

(51) Brouwers, J.; Brewster, M. E.; Augustijns, P. Supersaturating Drug Delivery Systems: The Answer to Solubility-Limited Oral Bioavailability? *J. Pharm. Sci.* **2009**, *98*, 2549–2572.

(52) Berben, P.; Brouwers, J.; Augustijns, P. The Artificial Membrane Insert System as Predictive Tool for Formulation Performance Evaluation. *Int. J. Pharm.* **2018**, *537*, 22–29.

(53) Stewart, A. M.; Grass, M. E.; Brodeur, T. J.; Goodwin, A. K.; Morgen, M. M.; Friesen, D. T.; Vodak, D. T. Impact of Drug-Rich Colloids of Itraconazole and HPMCAS on Membrane Flux in Vitro and Oral Bioavailability in Rats. *Mol. Pharm.* **2017**, *14*, 2437–2449.

(54) Kesiosoglou, F.; Wang, M.; Galipeau, K.; Harmon, P.; Okoh, G.; Xu, W. Effect of Amorphous Nanoparticle Size on Bioavailability of Anacetrapib in Dogs. *J. Pharm. Sci.* **2019**, *108*, 2917–2925.

(55) Mosquera-Giraldo, L. I.; Li, N.; Wilson, V. R.; Nichols, B. L. B.; Edgar, K. J.; Taylor, L. S. Influence of Polymer and Drug Loading on the Release Profile and Membrane Transport of Telaprevir. *Mol. Pharm.* **2018**, *15*, 1700–1713.

(56) Alonzo, D. E.; Gao, Y.; Zhou, D.; Mo, H.; Zhang, G. G. Z.; Taylor, L. S. Dissolution and Precipitation Behavior of Amorphous Solid Dispersions. *J. Pharm. Sci.* **2011**, *100*, 3316–3331.

(57) Ueda, K.; Taylor, L. S. Polymer Type Impacts Amorphous Solubility and Drug-Rich Phase Colloidal Stability: A Mechanistic Study Using Nuclear Magnetic Resonance Spectroscopy. *Mol. Pharm.* **2020**, *17*, 1352–1362.

(58) Ueda, K.; Yamamoto, N.; Higashi, K.; Moribe, K. Molecular Mobility Suppression of Ibuprofen-Rich Amorphous Nanodroplets by HPMC Revealed by NMR Relaxometry and Its Significance with Respect to Crystallization Inhibition. *Mol. Pharm.* **2019**, *16*, 4968–4977.

(59) Adamson, A. W.; Gast, A. P. *Physical Chemistry of Surfaces*; Wiley: New York, 1967.

(60) Liu, X. Y. Interfacial Effect of Molecules on Nucleation Kinetics. *J. Phys. Chem. B* **2001**, *105*, 11550–11558.

(61) Davis, S. S.; Hardy, J. G.; Fara, J. W. Transit of Pharmaceutical Dosage Forms through the Small Intestine. *Gut* **1986**, *27*, 886–892.

(62) Appel, L. E.; Babcock, W. C.; Friesen, D. T.; Ray, R. J.; Smithey, D. T.; Shamblin, S. L.; Shanker, R. M. Pharmaceutical Dosage Forms Comprising a Low-Solubility Drug and a Polymer. U.S. Patent 9,445,998 B2, Sept 20, 2016.

(63) Friesen, D. T.; Shanker, R.; Crew, M.; Smithey, D. T.; Curatolo, W. J.; Nightingale, J. A. S. Hydroxypropyl Methylcellulose Acetate Succinate-Based Spray-Dried Dispersions: An Overview. *Mol. Pharm.* **2008**, *5*, 1003–1019.

(64) Curatolo, W.; Nightingale, J. A.; Herbig, S. M. Utility of Hydroxypropylmethylcellulose Acetate Succinate (HPMCAS) for Initiation and Maintenance of Drug Supersaturation in the GI Milieu. *Pharm. Res.* **2009**, *26*, 1419–1431.

(65) Tanno, F.; Nishiyama, Y.; Kokubo, H.; Obara, S. Evaluation of Hypromellose Acetate Succinate (HPMCAS) as a Carrier in Solid Dispersions. *Drug Dev. Ind. Pharm.* **2004**, *30*, 9–17.

(66) Van Speybroeck, M.; Mols, R.; Mellaerts, R.; Thi, T. D.; Martens, J. A.; Humbeek, J. V.; Annaert, P.; Mooter, G. V. d.; Augustijns, P. Combined Use of Ordered Mesoporous Silica and Precipitation Inhibitors for Improved Oral Absorption of the Poorly Soluble Weak Base Itraconazole. *Eur. J. Pharm. Biopharm.* **2010**, *75*, 354–365.

(67) Konno, H.; Taylor, L. S. Influence of Different Polymers on the Crystallization Tendency of Molecularly Dispersed Amorphous Felodipine. *J. Pharm. Sci.* **2006**, *95*, 2692–2705.

(68) Raina, S. A.; Zhang, G. G. Z.; Alonzo, D. E.; Wu, J.; Zhu, D.; Catron, N. D.; Gao, Y.; Taylor, L. S. Impact of Solubilizing Additives on Supersaturation and Membrane Transport of Drugs. *Pharm. Res.* **2015**, *32*, 3350–3364.

(69) Warren, D. B.; Benameur, H.; Porter, C. J. H.; Pouton, C. W. Using Polymeric Precipitation Inhibitors to Improve the Absorption of Poorly Water-Soluble Drugs: A Mechanistic Basis for Utility. *J. Drug Targeting* **2010**, *18*, 704–731.

(70) Schram, C. J.; Beaudoin, S. P.; Taylor, L. S. Impact of Polymer Conformation on the Crystal Growth Inhibition of a Poorly Water-Soluble Drug in Aqueous Solution. *Langmuir* **2015**, *31*, 171–179.

(71) Chen, Y.; Liu, C.; Chen, Z.; Su, C.; Hageman, M.; Hussain, M.; Haskell, R.; Stefanski, K.; Qian, F. Drug-Polymer-Water Interaction and Its Implication for the Dissolution Performance of Amorphous Solid Dispersions. *Mol. Pharm.* **2015**, *12*, 576–589.